International Journal of Speleology	49 (3)	173-186	Tampa, FL (USA)	September 2020

Available online at scholarcommons.usf.edu/ijs

International Journal of Speleology

Official Journal of Union Internationale de Spéléologie

Bubble trail and folia in cenote Zapote, México: petrographic evidence for abiotic precipitation driven by CO_2 degassing below the water table

Rafael López-Martínez [1*], Fernando Gázquez [2], José M. Calaforra [2], Philippe Audra [3], Jean Y. Bigot [4], Teresa Pi Puig[5], Rocío J. Alcántara-Hernández [5], Ángel Navarro[6], Philippe Crochet[7], Liliana Corona Martínez [8], and Raquel Daza Brunet [1]

[1]Carbonate and Karst Process Laboratory, Institute of Geology, Av. Universidad 3000, National Autonomous University of México, Coyoacán, México City, 04510, México
[2]Water Resources and Environmental Geology, University of Almeria, La Cañada de San Urbano s/n, 04120 Almeria, Spain
[3]Université Nice Côte d'Azur, Polytech'Lab, 930 route des Colles, 06903 Sophia-Antipolis, Nice, France
[4]21 Rue des Hospices, 34090 Montpellier, France
[5]National Laboratory of Geochemistry and Mineralogy, Institute of Geology, Av. Universidad 3000, National Autonomous University of México, Coyoacán, México City, 04510, México
[6]The Gopro Family, Quintana Roo, Playa del Carmen, Quintana Roo, México
[7]Photographe de la spéléologie et du monde minéra, 145 cour Watt, 34000 Montpellier, France
[8]Centro de Geociencias (CGEO), National Autonomous University of México, Juriquilla Campus, Blvd. Juriquilla 3001, Querétaro, 76230, México

Abstract: Folia are speleothems that resemble bells, inverted cups, or bracket fungi, and whose origins are still controversial. Cenote Zapote (an underwater cave) in the Yucatán Peninsula (México), is home to some of the largest folia reported to date. These speleothems are currently growing in an active underwater system, meaning this site offers an excellent opportunity to constrain the different formation models proposed for folia, which have traditionally relied on inactive examples. In Cenote Zapote, folia are closely related to bubble trails and cupolas, suggesting an underwater CO_2-degassing process. In thin section, they display a succession of columnar-open and columnar-elongated endings in micrite-dendritic fabrics. Our petrographic and geochemical results demonstrate the abiotic origin of these folia and indicate carbonate precipitation from cold water by CO_2 degassing below the water table that started at least 5,210 yrs BP. We conclude that these folia formed as a result of subaqueous calcite precipitation around CO_2 bubbles trapped below overhanging walls of the cave. The sequential alternation of columnar and micritic fabrics can be explained by changes in the position of the halocline and H_2S-rich water mass while the exceptional size is the result of carbonate precipitation from waters saturated in $CaCO_3$ during thousans of years. Then we propose the classification of these speleothems as a subtype of folia. This subtype could be named Hells Bells, respecting its original description.

Keywords: folia, bubble trails, karst, cenote, underwater caves, speleothems, Hells Bells

Received 13 August 2020; Revised 4 October 2020; Accepted 5 October 2020

Citation: López-Martínez R., Gázquez F., Calaforra J.M., Audra P., Bigot J.Y., Pi Puig T., Alcántara-Hernández R.J., Navarro Á., Crochet P., Corona Martínez L. and Daza Brunet R., 2020. Bubble trail and folia in cenote Zapote, México: petrographic evidence for abiotic precipitation driven by CO_2 degassing below the water table. International Journal of Speleology, 49 (3), 173-186. Tampa, FL (USA) ISSN 0392-6672 https://doi.org/10.5038/1827-806X.49.3.2344

INTRODUCTION

The origin of folia speleothems is still a matter of debate among karst researchers (Kolesar & Rigg, 2004; Audra et al., 2009; Queen, 2009; Davis, 2012; Stinnesbeck et al., 2018). Folia speleothems typically resemble inverted rimstone dams, inverted cups, bells, or bracket fungi growing downwards (Hill & Forti, 1997; Audra et al., 2009; Davis, 2012) (Fig. 1) and have been reported in at least 30 caves worldwide (e.g., Audra et al., 2009; Davis, 2012; Gázquez & Calaforra, 2013; D'Angeli et al., 2015). They often appear close to other subaqueous speleothems, including calcite rafts, mammillary crusts, calcite raft cones, and "mushrooms" (Gázquez & Calaforra, 2013; D'Angeli et al., 2015). Even though most examples of folia have been reported in hypogenic, hydrothermal caves, there are also some cases described in epigenetic, cold-water caves (Plan & De Waele, 2001).

*ralopezm@geologia.unam.mx

The author's rights are protected under a Creative Commons Attribution-NonCommercial 4.0 International (CC BY-NC 4.0) license.

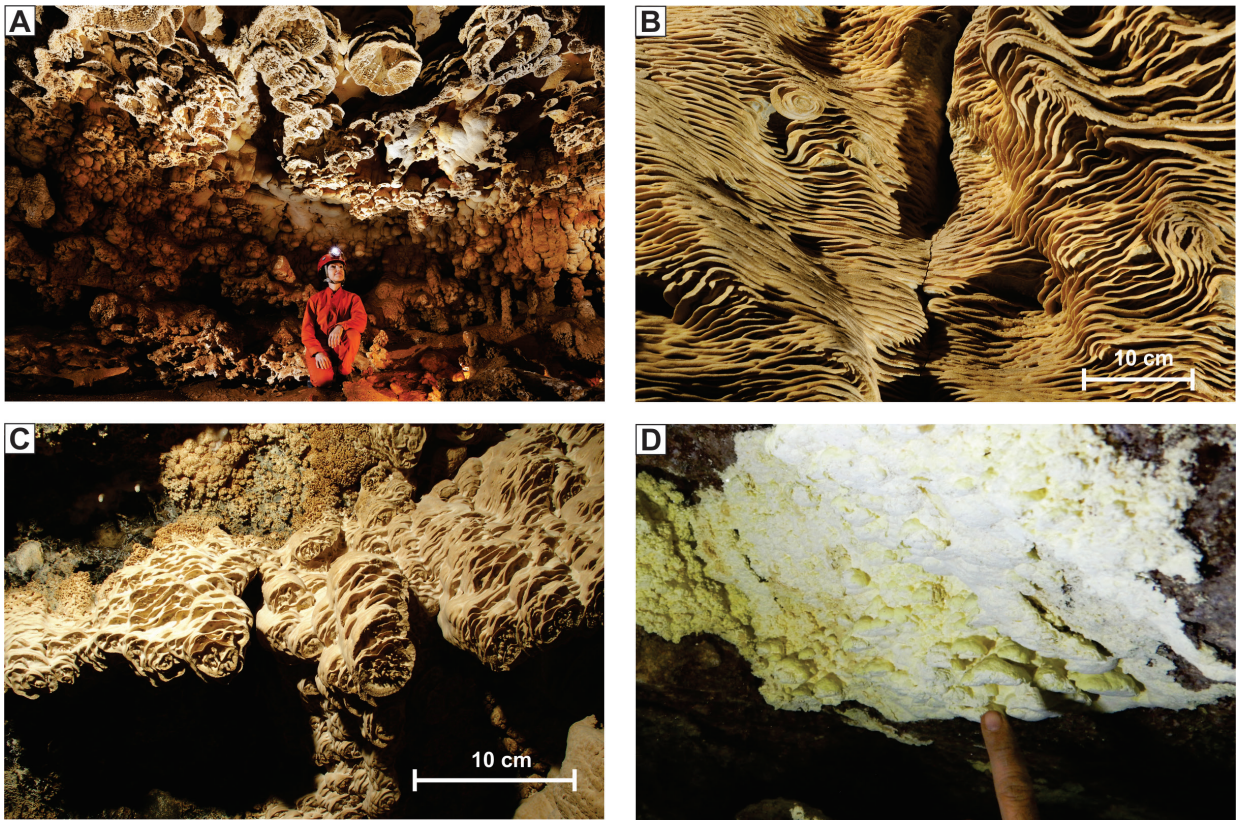

Fig. 1. Some examples of folia reported in caves around the world. A) Cueva de Santa Catalina, Cuba; B) Pal Volgyi Cave, Hungary (A–B photographs by Philippe Crochet); C) Sima de la Higuera (Murcia, Spain; photograph by Andrés Ros); D) Grotta Acqua Mintina (sulfur folia; photograph by Marco Vattano).

Past works

Though identification of folia is relatively simple because of their typical shape, the mechanisms involved in their genesis and classification are still controversial. Indeed, Audra et al. (2009) proposed that only calcite forms can be considered as real folia, while Davis (2012) includes a variety of shapes and mineral for the term. Despite most folia reported to date being made of calcite, some examples of folia composed of native sulfur have been described (Hose et al., 2000, 2009; Lugli et al., 2017; D'Angeli et al., 2018).

At present, two main models explain the formation of folia, including (1) precipitation at the air-water interphase as a "border" speleothem and (2) underwater formation througth CO_2 degassing, biologically, or other processes. Davis (1997, 2012) explained the growth of folia by accretion of particles at the air-water interface, including calcite precipitation brought about by CO_2 degassing and occasional evaporation. As such, the water level fluctuations determine the vertical distribution of the folia on the cave walls and ceilings. More recently, D´Angeli et al. (2015) provided robust geochemical and textural evidence for folia precipitation at the air-water interface as "border" speleothems in Santa Catalina Cave (Matanzas, Cuba). Their results also allowed the reconstruction of sea level variations and uplift rates in that region (De Waele et al., 2017, 2018). A similar approach was used to explain the formation of folia in the Devil's Hole (Nevada, USA) (Kolesar & Rigg, 2004).

In contrast, some authors have proposed a formation model for folia that involves subaqueous carbonate precipitation tens of centimetres to metres below the water surface. These include the underwater precipitation model proposed by Green (1991, 1997), later adopted by Audra et al. (2009) that conceives folia as subaqueous speleothems in the strict sense. In particular, Green (1991; 1997) claimed that the genesis of folia is directly related to the accumulations of CO_2 bubbles stemming from the degassing of thermal water that gets trapped by wall irregularities with calcite precipitation downwards around the bubble-water interface. A similar approach was used by Audra et al. (2009) to interpret the formation of folia and bubble pockets in Grotte de l'Adaouste (Provence, France) as well as in other caves worldwide. These authors highlighted the importance of cave wall geometry, as it plays a decisive role in controlling the genesis of folia.

As the debate is still ongoing, Davis (2012) challenged the scientific community to find (1) active folia sites with evidence of deeper bubble degassing (to rule out the possibility of surface degassing) and (2) brine/fresh-water mixing environments with no precipitation of calcite rafts. Here we present field and petrographic folia results from Cenote Zapote (Yucatán Peninsula, México) that fulfill these requirements. These speleothems were first studied by Stinnesbeck et al. (2018), who developed a genetic model based on biological-mediated processes (excellent videos about diving in Cenote Zapote are available at: https://www.youtube.com/watch?v=28qQzQ36sXc).

Although these authors did not refer explicitly to the term folia, their morphologies match those of folia speleothems. We aim to (1) demonstrate the abiotic origin of folia in Cenote Zapote speleothems and (2) shed light on the general genetic model of folia and their relationship with bubble trails.

GEOLOGICAL SETTINGS AND SITE DESCRIPTION

The Yucatán Peninsula is a shallow carbonate platform composed of a >3000 m thick limestone sequence (López-Ramos, 1983; Ward et al., 1985, 1995). The whole peninsula has been affected by intense karstification processes, resulting in a high density of karst systems, including the most extensive underwater caves in the world (Sac Actun Cave is 368 km in length) (https://caves.org/project/qrss/qrlongesp.htm).

The genesis and enlargement of these caves came about as a result of two speleogenetic processes: dissolution at the halocline (seawater-freshwater mixing) (Beddows, 2004; Smart et al., 2006) and oxidation of organic carbon (Gulley et al., 2016). Cenote Zapote (Fig. 2) is a typical vertical pit-cenote, about 20 km inland in Quintana Roo state, México. It was first surveyed by Vicente Fito, who discovered the speleothems and named them as "*Hells Bells*" (Stinnesbeck et al., 2017).

The cenote is about 60 m deep (50 m infilled by water) with an "hourglass" shape. A narrow vertical conduit connects two large voids, and no horizontal passages exist. In the central part, there is a massive accumulation of debris, as a result of the roof collapsing, accompanied by a large amount of organic matter, including leaves and remains of an ancient ceiba tree (*Ceiba pentandra*) dated to 3,568–3,453 cal yr BP (Stinesbeck et al., 2018).

Cenote Zapote hosts a stagnant water body with a stratified water column that can be divided from top to bottom into fresh oxygenated water (0–30 m); brine water with a sulfide cloud (30–40 m) and briny oxygen-depleted waters at the bottom (40–50 m). A detailed description of the water chemistry can be found in Stinnesbeck et al. (2018) and Ritter et al. (2019). Folia appear at a depth ranging from ~29 to ~36 m, but some initial stages of growth were documented at ~39 m.

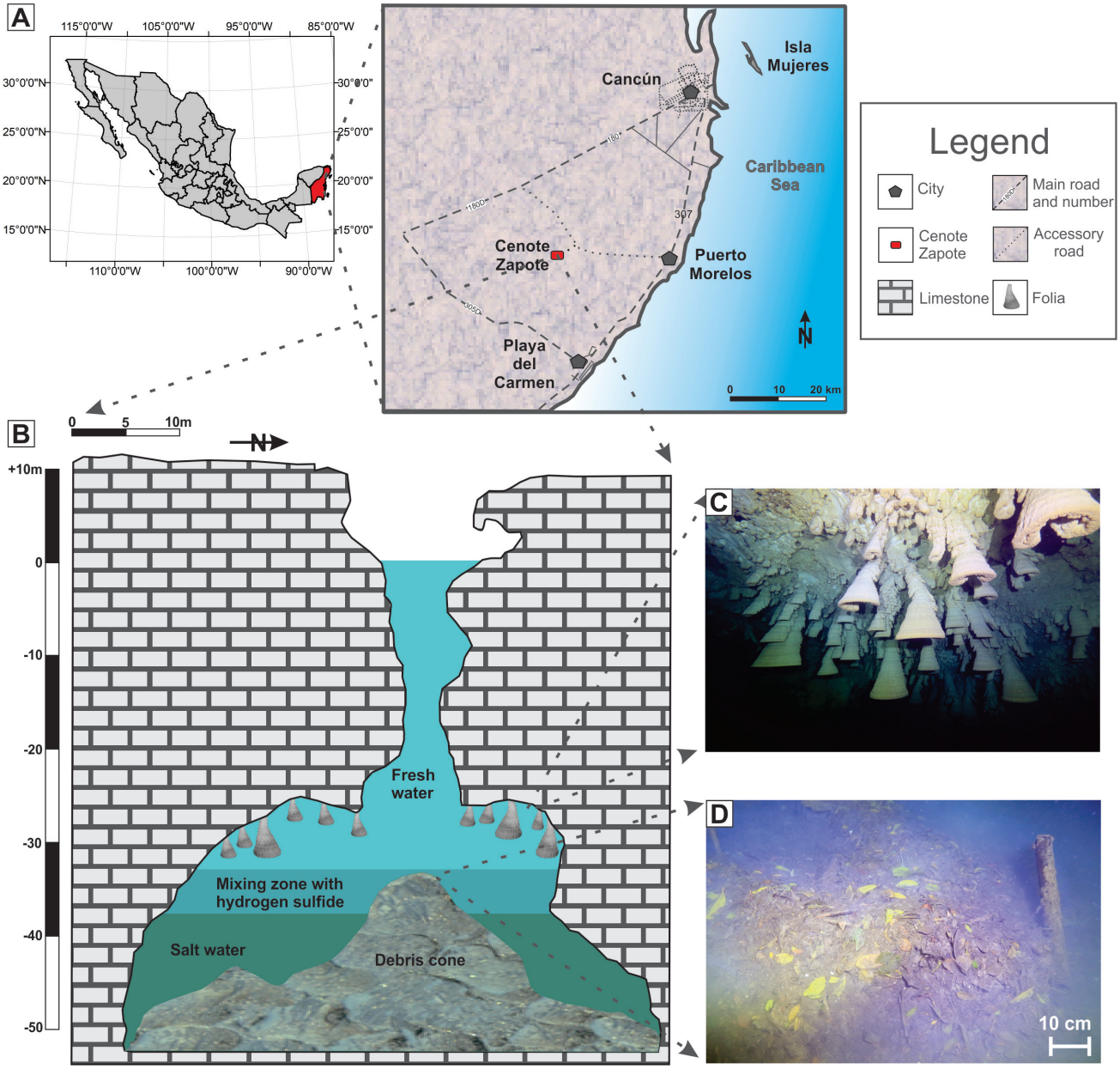

Fig. 2. A) Location and map of Cenote Zapote in the Yucatan Peninsula. Cenote Zapote is located near Puerto Morelos in the Mayan "Ruta de los Cenotes"; B) Note the hourglass shape of the cenote and the water-column stratification, including the mixing zone with hydrogen sulfide; C) General view of the folia on the overhanging wall; D) The bottom is covered with an extensive debris cone of organic matter, including leaves and wood, which is the source of the hydrogen sulfide. The map of the cenote was modified from Stinnesbeck et al. (2017).

METHODS

Documentation and sampling of the folia were conducted in July 2015 with typical cave diving procedures. Three small samples of the folia at different growth stages were taken from non-visible locations to avoid deterioration of the cave. Morphologies and structures were measured *in situ* and documented by photography and video.

Petrography and mineralogy

We analyzed longitudinal and cross thin-sections of samples under an Olympus BX51 microscope. In addition, thin sections were examined under epifluorescence of 590 nm for the detection of organic compounds such as fulvic acids (van Beynen et al., 2001; Brennan & White, 2013). For the description of fabric, we adopted the terminology of Frisia et al. (2000) and Frisia (2014), whereas for layer boundaries we used the terminology of Railsback et al. (2013).

We selected four samples (Fig. 3) at different stages of folia growth for mineralogical analysis by powder X-ray diffraction at the National Laboratory of Geochemistry and Mineralogy (LANGEM), part of the Institute of Geology, National Autonomous University of México (UNAM), México. We used an EMPYREAN XRD diffractometer operating with an accelerating voltage of 45 kV and a filament current of 40 mA, using CuKα radiation, nickel filter, and PIXcel 3D detector. The sample was scanned in the 2θ angle range of 4-70° measured with a step size of 0.04° (2θ) and 40 s scan step time. The diffraction patterns were analyzed with version 4.5 of the HighScore program with reference patterns from the ICDD PDF-2 and ICSD databases.

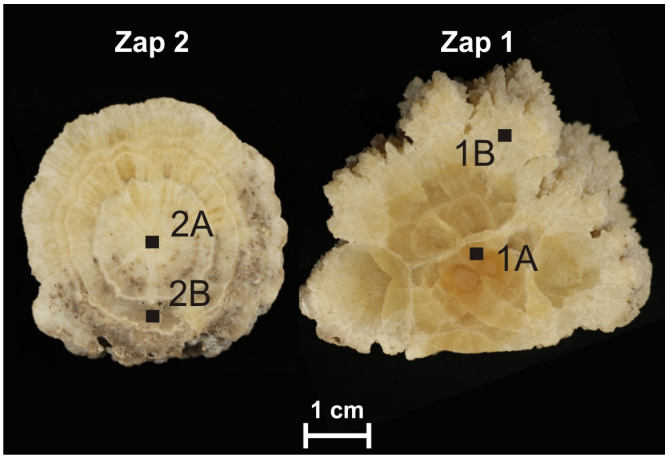

Fig. 3. Position of the samples used for X-ray diffraction and stable isotope analysis. Zap 2 represents the initial growing phase, whereas Zap 1 shows the well-developed crystals. Sample Zap 2A was selected for U/Th dating.

Geochemical analyses

Four powder subsamples (~0.9 mg) were extracted from sample Zap1 and Zap2 using a micro drill (Fig. 3) and analysed for stable carbon and oxygen isotopes ($\delta^{13}C_{carb}$ and $\delta^{18}O_{carb}$) at the National Laboratory of Geochemistry and Mineralogy (LANGEM), part of the Institute of Geology, National Autonomous University of México (UNAM), México. The carbonate was reacted with orthophosphoric acid at 25°C for 54 h under vacuum conditions following the guidelines of McCrea (1950). After that, the released CO_2 was analysed by a Thermo Finnigan MAT 253 mass spectrometer coupled with a Gas Bench II. Results are reported in per mil versus V-PDB (Vienna Pee Dee Belemnite) with reproducibility within 0.2‰ for $\delta^{13}C_{carb}$ and $\delta^{18}O_{carb}$.

The age of the inner part of sample Zap 2A (Fig. 3) was determined by U-Th dating, using a Thermo-Finnigan Neptune Plus at Centro de Geociencias, Juriquilla Campus, UNAM (Querétaro, México), following the conventional method described elsewhere (McCulloch & Mortimer, 2008; Hernández-Mendiola et al., 2011).

RESULTS

Morphologies

Bubble trails and cupolas

Bubble trails were first recognized in the karst literature by Chiesi & Forti (1987) and are closely related to folia (Audra et al., 2009). They are small subaqueous channels carved into the carbonate host rock of the cave wall, as a result of dissolution due to the rise of CO_2 bubbles (Audra et al., 2009). In Cenote Zapote, some morphologies are the result of such a process, including bubble trails, and cupolas (Fig. 4).

Morphologies vary from certain structures resembling inverted *rillenkarren, trittkarren*, and *kamenitza* (Fig. 4A-C) to channels (Fig. 4C-E) (see examples of these structures in subaereal conditions in picture 4.11, page 48, and picture 4.46, page 135 of Veress, 2010). Channels are straight to slightly curved depending on irregularities and variation of the slope of the overhanging walls. Width generally decreases upwards, with a maximum of 25 cm. Fig. 4C shows the relationship between bubble trails and cupolas in Cenote Zapote, where small channels (arrow 1) feed a cupola (arrow 2). Beyond the point where the cupola cannot store all the gas supplied by these feeding channels, a decantation runnel allows the excess gas to escape (arrow 3).

Folia

In Cenote Zapote, folia occur on the overhanging walls (Fig. 2), and their lengths vary from 1-2 cm to up to 2 m. Their cross-sections can be seen as arch shapes with various degrees of amplitude (Fig. 5A, B). Nonetheless, they do not grow around the entire circumference from the beginning, as displayed in Fig. 5C, where 1-5 represent different stages of growth.

Initially, folia growth starts as an inverted "*knobby stalagmite*" (Fig. 5C). As it continues growing, it develops a "*stem*" (Fig. 5D). After that, the outer part of the stem grows faster while the inner is laggard, leading to the formation of an apex. During the last formation stage, well-developed crystals precipitate on the surface, very similar to phreatic overgrowth (Fig. 5D). Generally, well-developed folia display a composite pattern, with numerous small folia growing over bigger ones (Fig. 5E). Note that moving up the wall, folia decrease in size until they disappear. They also tend to be flatter in shape. (Fig. 5F).

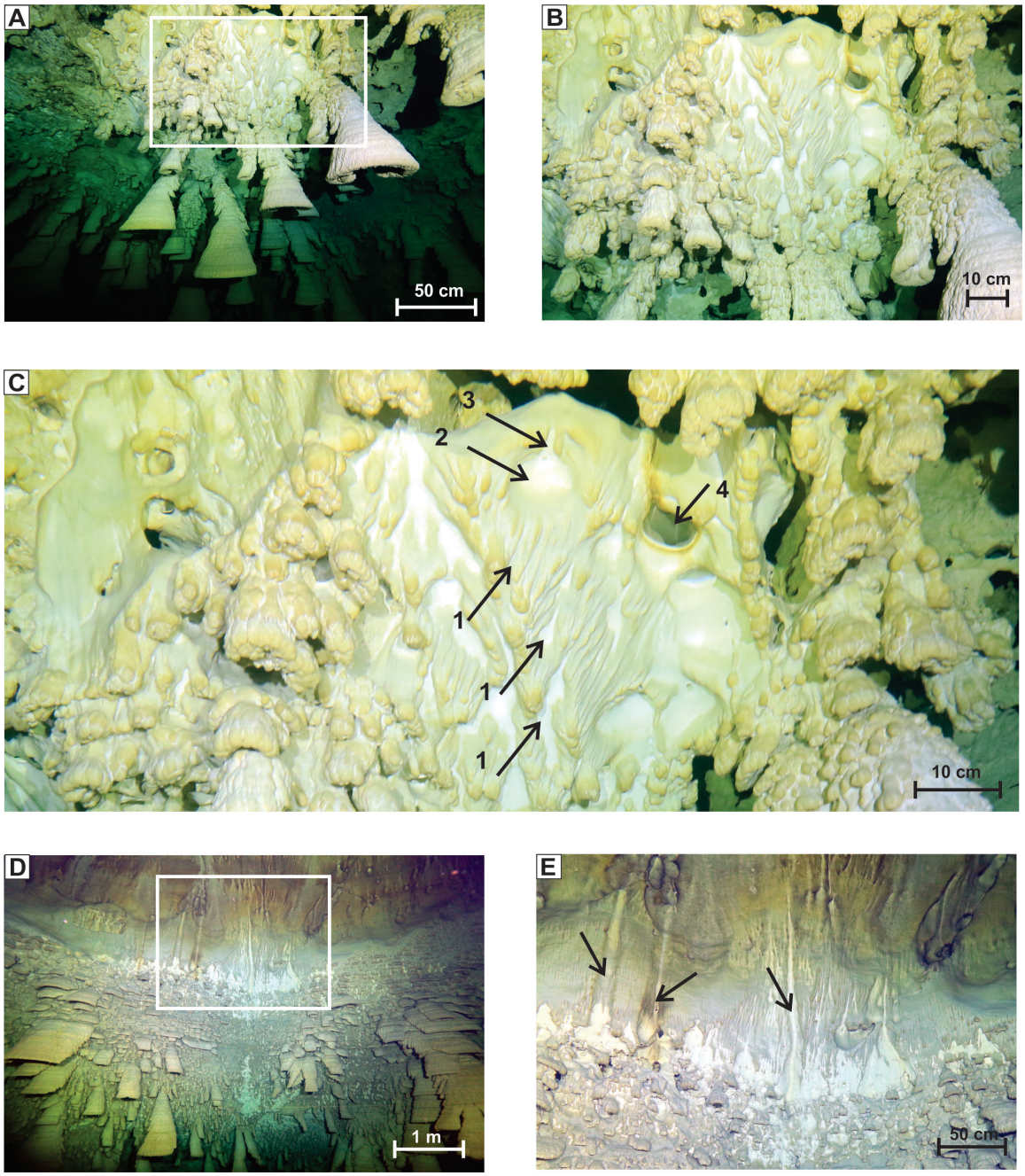

Fig. 4. Morphologies of bubble trails. A) General view of the relationship between folia and bubble trails; B) Detailed view of picture A. Note the similarity between the inverted rillenkarren, trittkarren and kamenitza; C) Morphologies of bubble trails and their relationship with cupolas. Arrow 1 denotes bubble trails feeding a cupola (arrow 2) and arrow 3 points to a decantation runnel which allows the excess gas to escape. Arrow 4 indicates a gas bubble product of the diving activity; D–E) Details of the bubble trails on the upper part of the roof (see arrows). Note that moving up the wall, the folia size decreases, until only bubble-trails appear.

Textural observations and mineralogy

The studied folia display irregular alternate banding of white (spar) and dark (micrite) laminae (Fig. 6A, B). In the longitudinal section, laminae are thick along the growth axis and become thinner to both sides (Fig. 6A). This part of the stem resembles a stalagmite, although the first can be observed in the cross-section of the apex (Fig. 6B). Here, the first steps of speleothem growth show a "flower" pattern with multiple nucleation centers and the first steps of preferential growth in one direction. Small dots, mainly concentrated in the micritic parts, are made of pyrite (FeS_2) and siderite ($FeCO_3$), as confirmed by XRD analyses (Table 1).

The growth succession starts with columnar-open fabric, continues with columnar-elongated, and ends with micritic-dendrite fabric (Fig. 6C). The columnar-open fabric displays a series of well-formed calcite crystals with different orientations and high inter-crystalline porosity (Figs. 6D, E, 8A). Under epifluorescence, the crystals exhibit bands with different degrees of fluorescence (Fig. 6E). We observed that the crystals display flat-convex surface terminations (Fig. 8B, arrows 1 and 2). These terminations are typical of growth at an air-water interface along which the air limits the development of crystals (e.g., Kovacs et al., 2017b).

The columnar-open fabric to columnar-elongated *(Ce)* fabric transition displays large calcite crystals following a preferential growth direction and some slightly divergent crystallites (Fig. 7A). This fabric exhibits blade termination (Fig. 7B) covered with

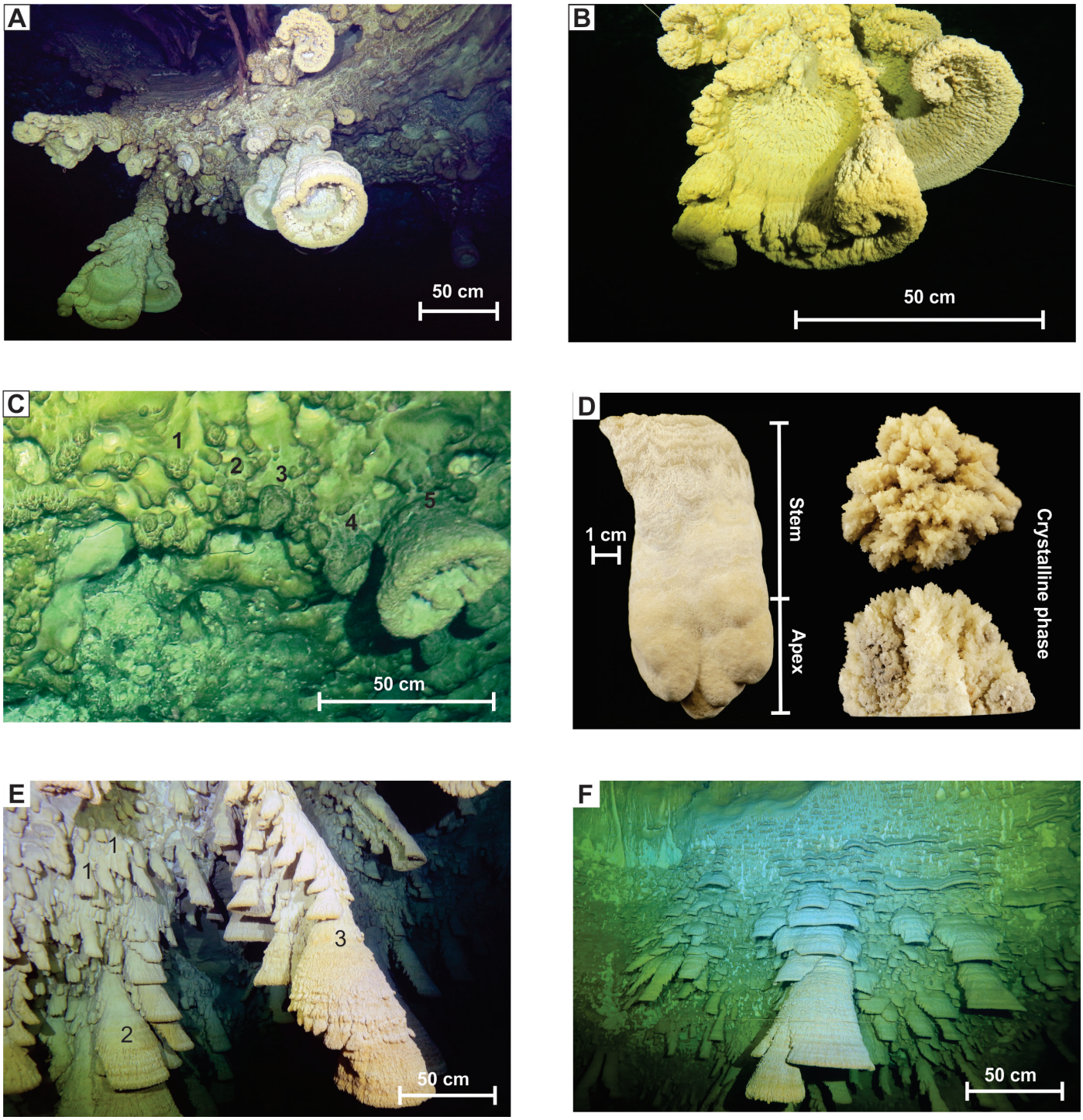

Fig. 5. Details of folia morphologies. A) Vertical downward view. Note the different morphologies from full circumference to semi-circumference with coiling edges; B) Features of the typical folia resembling inverted rimstone; C) Various growth stages of folia (1-5) starting from a "*knobby stalagmite*" and finishing in a well-developed circular folia. Some cupolas are full of gas; D) Details of the first stages of the folia. On the left side is the stem and apex of the folia, while on the right is the crystalline phase; E) Folia speleothems at different development stages. Number 1 indicates the "*knobby*" part with apex development, whereas 2 shows the full folia in the crystalline phase, and 3 shows a composite type, with small folia using the bigger ones as a substrate. Note that folia grow in the opposite direction to the substrate, which can be the wall or other folia; F) Higher up the wall, the folia decrease in size, and their shapes tend to be flatter. Scales are approximate due to various depths of field in photos in A, B, C, E, and F.

Table 1. Mineralogical and isotopic composition of the studied samples.

	Calcite (%)	**Siderite (%)**	**Quartz (%)**	**Pyrite (%)**	**$\delta^{13}C$ (‰)**	**$\delta^{18}O$ (‰)**
Zap 1A	99.5	-	0.5	-	–12.5	–5.2
Zap 1B	100	-	-	-	–12.7	–5.1
Zap 2A	99.1	0.9	-	-	–12.4	–5.2
Zap 2B	>99	Traces	Traces	Traces	–11.9	–5.3

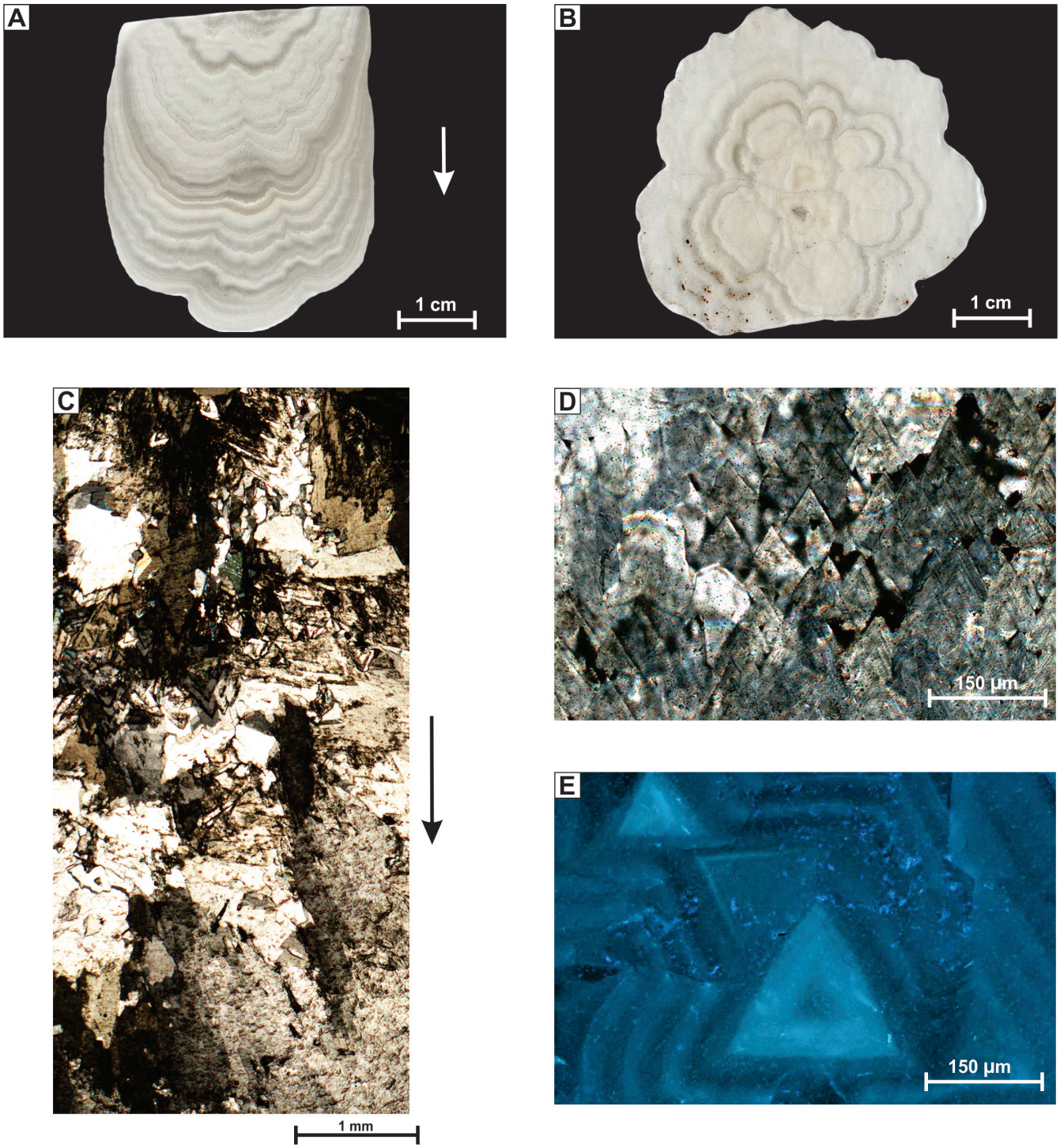

Fig. 6. Petrography of the folia from Cenote Zapote. The arrow indicates the growth direction. A) A longitudinal cut through the stem of the folia. The light laminae are formed of spars, while the dark ones are micrite. Note how the laminae are thicker in the growth axis and thinner to the sides, similar to stalagmites; B) Cross-section of the apex. Small dots of pyrite and siderite appear within the micritic bands; C) Evolution of the calcite fabrics from columnar-open to columnar-elongated and finally micritic-dendrite fabric. The arrow indicates the growth direction; D) Columnar-open fabric under planar polarization; E) The same fabric subject to epifluorescence of 590 nm. Note the different fluorescence grades related to the presence of organic substances with low molecular weight.

a dark micritic fabric *(M)*. The elongated columnar and micrite displays a Type-E contact (dissolution-erosion), according to Railsback et al. (2013), with the presence of micro-cavities (Fig. 6C) and coated particles along the border (Fig. 7D).

The micrite fabric is dark under plane polarization and is variable in width, from very thin (as in Fig. 7B) to a more developed band. This is a result of a destructive process of micritization of the previous fabric (mainly elongated columnar). Micrite is more luminescent under UV light, suggesting the presence of soil-derived organic compounds (e.g., fulvic acid) at the time of formation. Within the micrite layer, some examples of dendritic fabric *(D)* with typical scaffold-like morphology have been found (Figs. 7H, 8C, D). In places, the formation of *in situ* micrite (particle size less than 2µm) from the destruction of columnar fabric can be observed (Fig. 8D-F).

Geochemical analyses

The $\delta^{13}C_{VPDB}$ values of the studied samples range from –11.9 to –12.7‰, whereas the $\delta^{18}O_{VPDB}$ values vary from –5.1 to –5.3‰ (Table 1). The inner part of sample Zap2 2A is 5,210 ± 140 yr BP (Table 2).

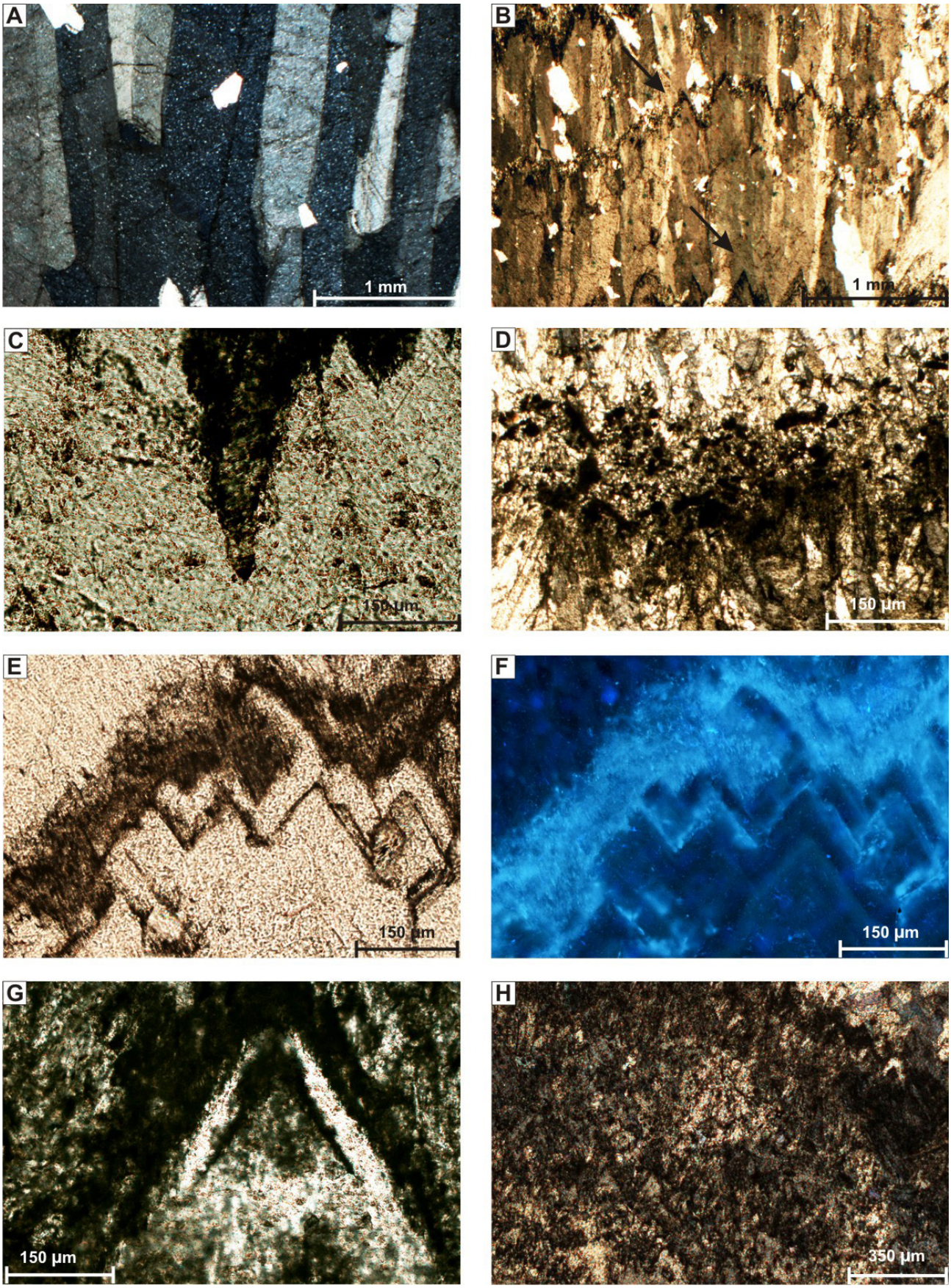

Fig. 7. Petrography of the folia from Cenote Zapote. A) Columnar-elongated fabric (cross-polarisation); B) The columnar-elongated fabric ends in a blade shape alternating with a micritic zone; C) Dissolution micro-cavities in contact with the columnar-elongated fabric and micrite zone; D) Coated particles along the contact between both fabrics; E–F) Contact between well-developed crystals and micrite viewed in plan polarized (E) and under epifluorescence (F) light. Note the micritization process is destroying the crystal. The epifluorescence shows a more fluorescent micrite due to the presence of organic compounds; G) Greater detail of the micritization process; H) Dendritic fabric with the typical scaffold-like morphology.

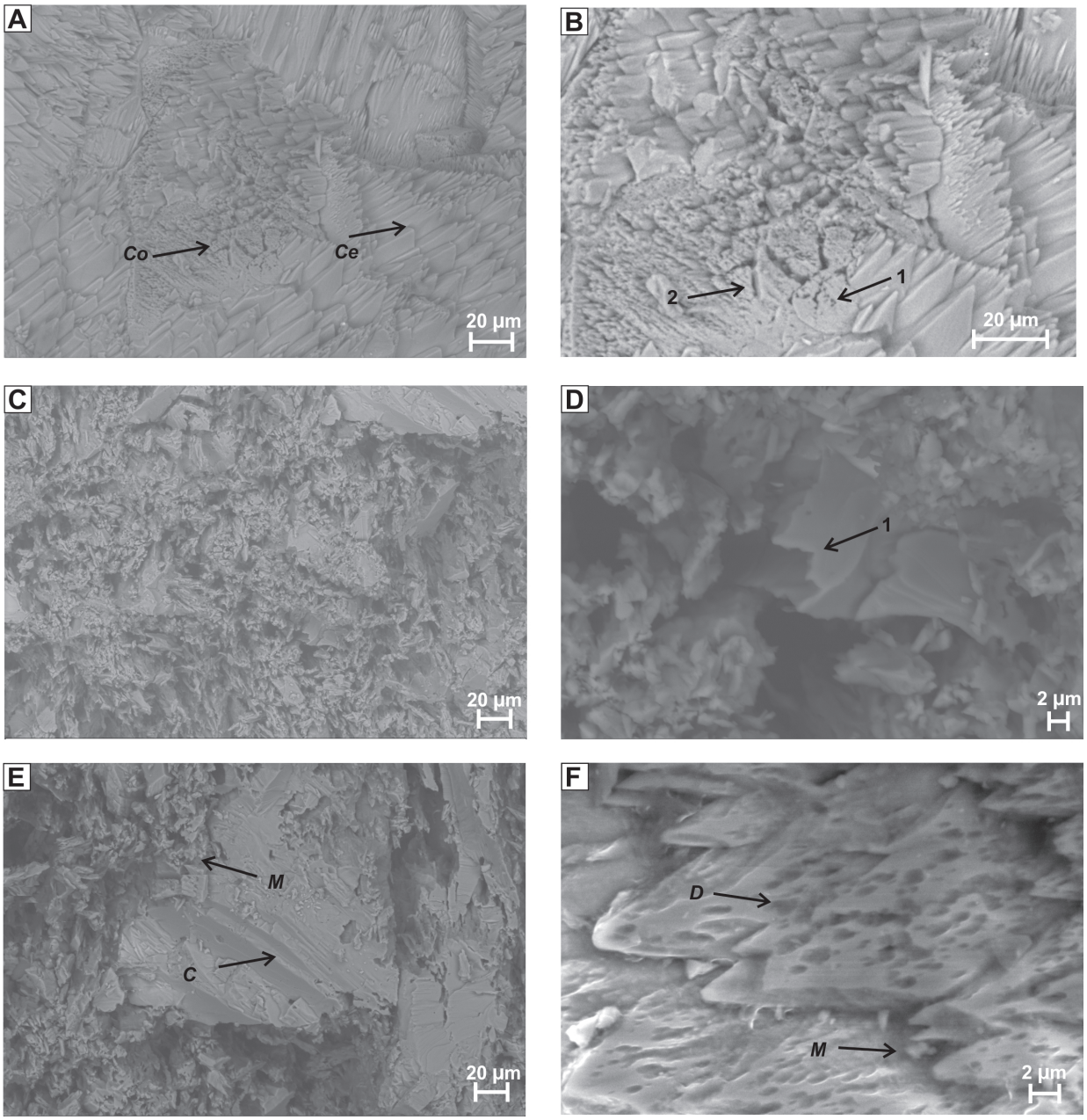

Fig. 8. SEM observation of the studied folia samples. A) General view of the columnar-open (*Co*) and columnar-elongated (*Ce*) fabrics; B) Details of the crystallites in the columnar-open fabric. Arrow 1 indicates the flat termination surface of the fabric, while arrow 2 shows a crystallite with convex shape growing from the near-flat surface; C) Micritic fabric with the details of the scaffold-like morphology; D) Broken edges of calcite crystals with the formation of *in situ* micrites (particle size less than 2 µm); E) The same process of micrite formation (*M*), starting from columnar fabrics (*C*); F) Details of dissolution features (*D*) in the columnar fabrics leading to the creation of micrite particles.

Table 2. U-Th dating data for sample Zap 2A.

Sample	^{238}U (ng/g)	^{232}Th (ng/g)	$^{230}Th/^{232}Th$ (activity)	$^{230}Th/^{238}U$ (activity)	$^{234}U/^{238}U$ (activity)	$\delta^{234}U_m$ (‰)	$\delta^{234}U_i$ (‰)	Age (ka) Uncorr.	Age (ka) Corr.
Zap 2A	644.8 ± 0.3	0.3913 ± 0.1004	252 ± 9	0.047 ± 0.001	1.02 ± 0.001	22.6 ± 1.3	23 ± 1.3	5.21 ± 0.14	5.19 ± 0.14

DISCUSSION

Bubble trails-folia connection and conditions for subaqueous calcite precipitation in Cenote Zapote

Previous studies suggested that all the folia formation stages in Cenote Zapote occurred underwater and that the vertical variations of the halocline is connected to regional recharge of the aquifer during storms which affected their growth (Ritter et al., 2019). However, these authors did not note the presence of bubble trails, which are closely related to folia formation in this cave.

Owing to hydrostatic pressure, CO_2 in underwater environments generally remains dissolved at depths >40 m (Audra et al., 2009). Once the pressure decreases, it tends to escape from solution and forms small bubbles. The CO_2 bubbles are channelled along bubble trails, move upwards, and dissolve the limestone cave walls, which releases the Ca^{2+} necessary for secondary carbonate precipitation. The CO_2 degassing from the bubbles occurs by diffusion to the water surrounding the bubble, triggering calcite precipitation along its edge. The flat-curved edge of some crystallites (Fig. 8B) is typical of crystals growing at the air-water interface

(e.g., calcite rafts; Kovacs et al., 2017b) and supports the hypothesis of calcite growth in connection with CO_2 bubbles. As a result, folia usually occur along the edges of bubble trails and cupolas (Fig. 9A, B) that are located below overhanging walls, as observed in other caves (Audra et al., 2009). No evidence for biologically-mediated calcite precipitation has been detected (e.g., mineralized microbes, stromatolitic structure, etc.; Jones, 2001), which means that the formation of folia in Cenote Zapote is an abiotic mechanism. This contrasts with previous studies that classified these folia as "*biothems*" (Stinnesbeck et al., 2018), which in our view, is not correct and agree with results of Ritter et al. (2019).

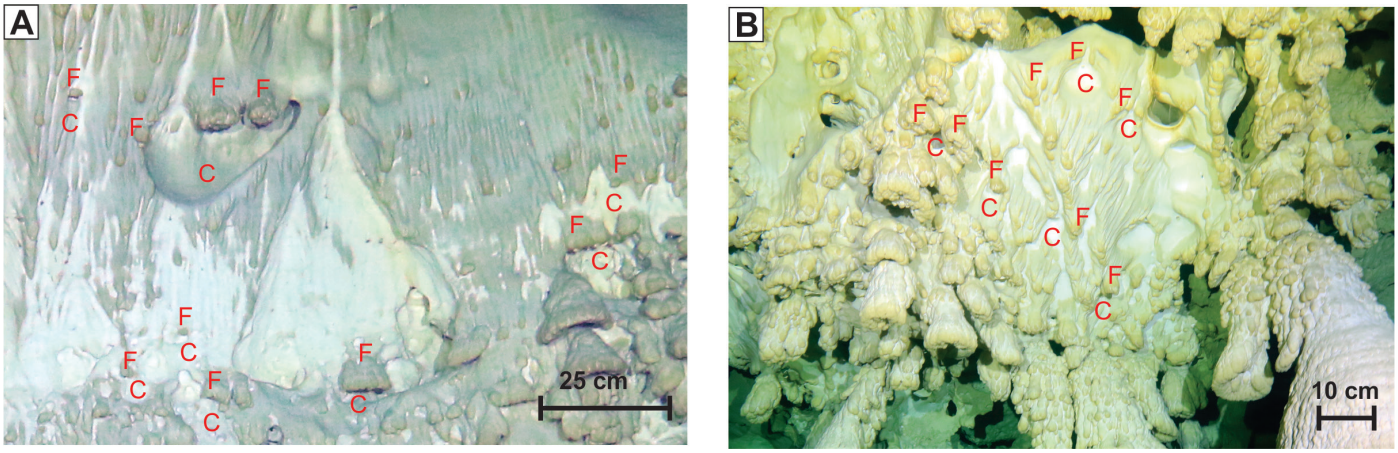

Fig. 9. Relationship between the growth of folia (F) and dissolution structures, including cupolas (C) and bubble trails. A-B) on the upper part of the wall, folia are scarce, and it is possible to observe the relationship more clearly. Folia appear more commonly on the upper part of the cupola, but small forms also appear to the sides of the bubble trails.

The $\delta^{18}O_{VPDB}$ values of the carbonate (–5.1 to –5.3‰) indicate that these speleothems precipitated from fresh-water ($\delta^{18}O_{water}$ ~–4 to –5‰, relative to the international standar V-SMOW) at a relatively low temperature (~20ºC) ruling out hydrothermal/hypogene calcite precipitation, that usually gives rise to lower $\delta^{18}O_{VPDB}$ values (e.g., Gázquez et al., 2018). In addition, the $\delta^{13}C_{VPDB}$ values (–11.9 to –12.7‰) indicate that the primary source of carbon for carbonate precipitation was the decay of organic matter, including the organic debris in the bottom and leaching from the soil above the cave, rather than CO_2 from hypogenic processes (Gázquez et al., 2018). Likewise, the $\delta^{234}U$ of 22.69 ± 1.34‰ does not point toward seawater contributions ($\delta^{234}U_{sea}$ of 146.8 ± 0.1‰; Andersen et al., 2010) during calcite precipitation, but crystallization from a fresh-water lens. Our U-Th dating results show that the Cenote Zapote folia grew at least as early as 5,210 ± 140 yr BP. Stinnesbeck et al. (2018) reported slightly younger ages (<4,500 yr BP) for the same speleothems. Accordingly, it is possible to extend the record of these folia by ~1,000 years.

Evolution model of folia formation

The evolution of the Cenote Zapote folia involves a complex mechanism that combines carbonate dissolution and precipitation. Initially, the roof of the cenote collapsed, allowing the input of a large amount of organic matter into the stagnant water. Organic matter oxidation led to the consumption of dissolved O_2 in the lower water lens and due to bacterial sulfate reduction processes, CO_2 and H_2S are produced. The CO_2 bubbles trapped in some wall irregularities produce a water-gas interface and CO_2 degassing, leading to calcite precipitation along the edges of the bubble in a tangential position (Fig. 10A, B). The studied samples display nucleation centres corresponding to the top of the bubble. This process also explains the circular shape of the folia.

On sub-vertical walls, the most efficient CO_2 degassing and calcite precipitation occurs in the outer part of the bubble (as opposed to the wall) because there is more space for crystal development (Fig. 10B). In contrast, bubbles trapped in an almost horizontal position develop without a preferential growth direction and display near-circular shapes (Fig. 10A). In summary, the morphology of the substrate on which folia form controls their shapes.

Subsequently, precipitation of columnar-open fabrics changes to columnar-elongated fabrics. The exposition of the columnar-open fabric to the calcium carbonate saturated fresh-water lens leads to the growth of large crystals typical of the columnar-elongated arrangement (Fig. 10F). This crystal development is interrupted by the periodic elevation of the halocline (Fig. 10G). During this time, the columnar fabrics are partially dissolved by calcium carbonate unsaturated water, which is slightly acidic because of the presence of H_2S. At this stage, micrite calcite forms. As evidenced by the luminescence, soil-derived compounds are incorporated into the calcite at this stage, which are probably more abundant in the water lens under the halocline. Additionally, this process occurs in oxygen-depleted water, leading to the precipitation of pyrite and siderite. The presence of pyrite and siderite within the micrite bands is a strong evidence that its formation is influenced by microbial activity in low-oxygen conditions similar to those described in marine environments (Wilkin et al., 1997; Wignall et al., 2010; Núñez-Useche et al., 2016; Martínez-Yañez et al., 2017). Once the mixing zone moves back to a deeper position, the micrite fabrics become exposed to the saturated fresh water lens and act as nucleation points for the development of new columnar fabrics (Fig. 9G), as observed elsewhere (Dickson, 1993).

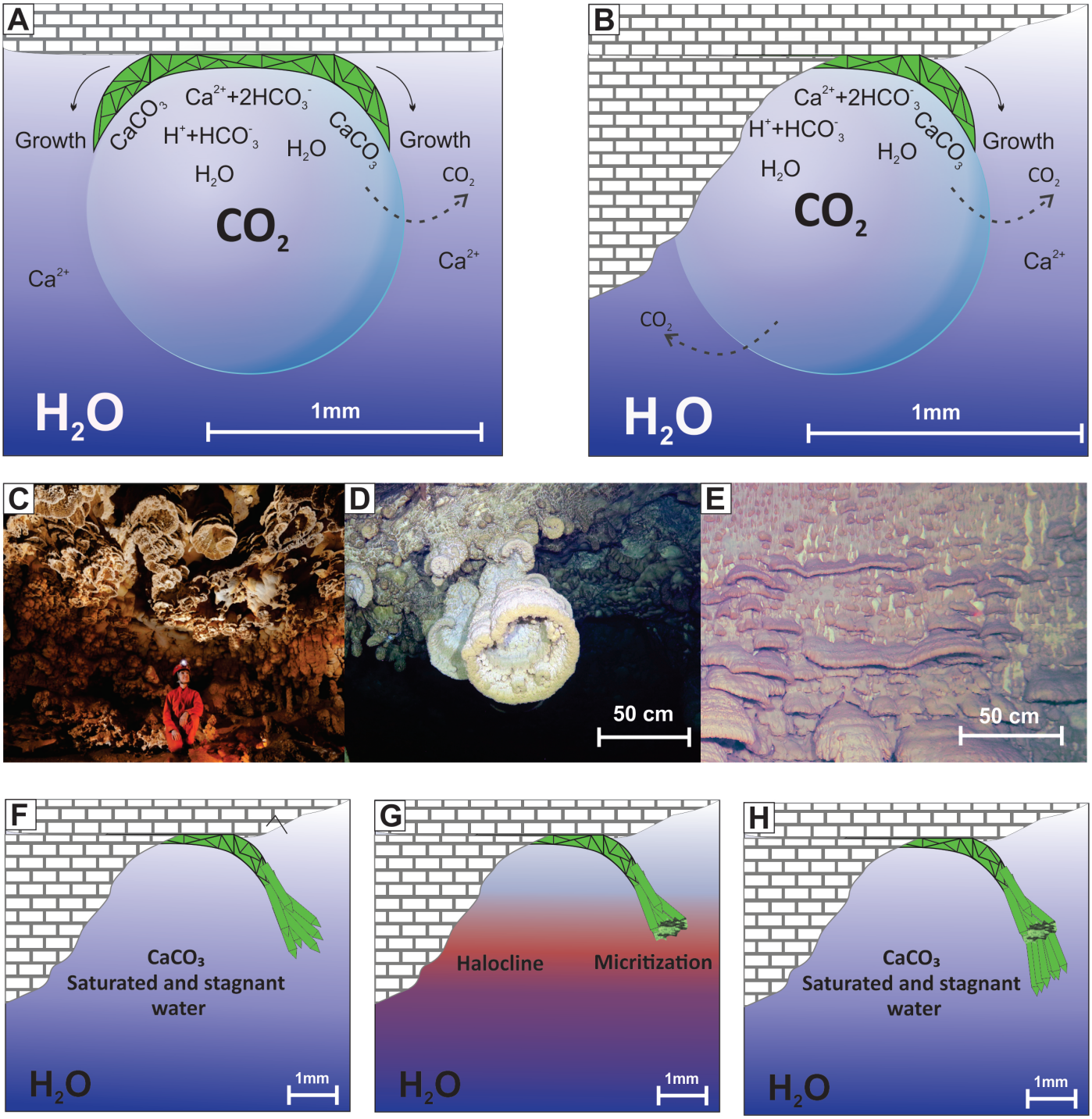

Legend

Columnar-open

Columnar-elongated

Micrite

Cave walls

Fig. 10. Genetic model of folia formation in Cenote Zapote and the calcite precipitation process occurring in the gas bubble, depending on the wall morphology. At this stage (A), the precipitation of the columnar-open fabrics occurs along the horizontal parts of walls. In this case, calcite crystals precipitate around the bubble, leading to the formation of circular folia; B) In sub-vertical walls, the calcite crystals tend to precipitate along the boundary of the bubble-wall zone; C-E) The shape of the folia is related to the wall inclination and morphology. It can vary from circular (C, D) to slightly flat (E); F) Once exposed to calcite saturated fresh water, the columnar elongated crystal grows out from the previous open-elongated. G. The rise of the halocline due to seasonal or sporadic events (e.g., storms or hurricanes) exposes the calcite crystals to non-saturated waters leading to dissolution. This process produces micrite fabrics; H) Once the halocline returns to normal levels, the micritic fabrics act as a precipitation nucleus for a new generation of columnar elongated calcitic fabric. The repetition of these process within saturated and stagnant waters allow the rapid growth and exceptional size of the folia in the Cenote Zapote.

CONCLUSIONS

The Cenote Zapote offers an excellent opportunity to view the constraints on the genesis of folia. Our morphological observations suggest that there is a close relationship between folia and bubble-trails, as previously proposed in hypogenic and eogenetic environments. Folia form in subaqueous conditions (tens of centimetres to metres below the water table) from calcite precipitation around CO_2 bubbles. The wall geometry plays a decisive role in controlling the shape of these speleothems.

The petrographic observations reveal abiotic calcite precipitation that includes a succession of columnar-open fabrics, columnar-elongated fabrics, and micritic fabrics. The columnar-open fabric corresponds to the first crystals precipitated along the edges of the gas bubble. The columnar-open fabrics changes to columnar-elongated as a result of being exposed to the calcium-carbonated saturated waters. The growth of columnar-elongated fabrics is interrupted and they are partially dissolved when the halocline rises. The crystals are subsequently exposed to calcium-carbonate unsaturated water, rich in H_2S that favours the formation of micritic fabrics. After that, because of the lowering of the halocline, the micrite is exposed once again to calcium carbonate saturated waters, leading to the growth of new columnar-elongated fabrics. The exceptional size of the folia in Cenote Zapote can be explained with the general model of folia plus some factors like the halocline position and special conditions of calcium-carbonate equilibrium. Then we propose to clasify these speleothems as a subtype of folia and preserve the original name of "Hells Bells".

ACKNOWLEDGMENTS

Funding for this research was provided by the National Geographic Society grant W418-15 and PAPIIT IN113020. We want to thank Santi Diving, Apeks, Ammonite Systems, and Casco Antiguo for sponsoring the diving gear. We wish to thank the "HIPATIA" research program at the University of Almería (F.G.). The present investigation was made possible due to the valuable support of Rosario Fátima of the Cenote Zapote and all the staff at the Zapote Ecopark. We also wish to thank Yuri Yerye and Salvador Trejo for their help during the underwater investigation and Andrés Ros for some photographs from Sima de la Higuera. We are grateful to Nick Stevenson who checked the language. This investigation was made possible through the PASPA program at the UNAM. We also thank Carol A. Hill, two anonymous reviewers, and Bogdan P. Onac for their revisions of the manuscript that enhanced the quality of the present publication.

Authorship statement: RLM, FG, JMC, and PA designed and directed the study. TPP, RA, and LCM conducted the analytical part of the study. JYB, AN, PC and RDB contributed in sampling and *in situ* documentation of the process. All authors contributed to the writing and discussion of the manuscript.

REFERENCES

Aubrecht, R., Brewer-Carías, C., Šmída, B., Audy, M., Kováčik, Ľ., 2008. Anatomy of biologically mediated opal speleothems in the World's largest sandstone cave: Cueva Charles Brewer, Chimantá Plateau, Venezuela. Sedimentary Geology, 203(3-4), 181-195. https://doi.org/10.1016/j.sedgeo.2007.10.005

Audra, P., Mocochain, L., Bigot, J.Y., Nobécourt, J.C., 2009. The association between bubble trails and folia: a morphological and sedimentary indicator of hypogenic speleogenesis by degassing, example from Adaouste Cave (Provence, France). International Journal of Speleology, 38(2), 93-102. https://doi.org/10.5038/1827-806X.38.2.1

Andersen, M.B., Stirling, C.H., Zimmermann, B., Halliday, A.N., 2010. Precise determination of the open ocean $^{234}U/^{238}U$ composition. Geochemestry, Geophysics, Geosystems, 11, 1-8. https://doi.org/10.1029/2010GC003318

Baker, A., Genty, D., Smart, P.L., 1998. High-resolution records of soil humification and paleoclimate change from variations in speleothem luminescence excitation and emission wavelengths. Geology, 26(10), 903-906. https://doi.org/10.1130/0091-7613(1998)026%3C0903:HRROSH%3E2.3.CO;2

Baker, A., Mockler, N.J., Barnes, W.L., 1999. Fluorescence intensity variations of speleothem-forming groundwaters: Implications for paleoclimate reconstruction. Water Resources Research, 35(2), 407-413. https://doi.org/10.1029/1998WR900057

Beddows, P.A., 2004. Groundwater hydrology of a coastal conduit carbonate aquifer: Caribbean coast of the Yucatán Peninsula, México. Unpublished Ph. Thesis, University of Bristol, 303 p.

Beddows, P.A., Smart, P.L., Whitaker, F.F., Smith, S.L., 2007. Decoupled fresh–saline groundwater circulation of a coastal carbonate aquifer: spatial patterns of temperature and specific electrical conductivity. Journal of Hydrology, 346(1-2), 18-32. https://doi.org/10.1016/j.jhydrol.2007.08.013

Bottrell, S.H., Smart, P.L., Whitaker, F., Raiswell, R., 1991. Geochemistry and isotope systematics of sulphur in the mixing zone of Bahamian blue holes. Applied Geochemistry, 6(1), 97-103. https://doi.org/10.1016/0883-2927(91)90066-X

Brennan, E.S., White, W.B., 2013. Luminescence of speleothems: a comparison of sources and environments. Journal of Cave and Karst Studies, 75(3), 210-217. https://doi.org/10.4311/2012ES0280

Caddeo, G.A., Railsback, L.B., De Waele, J., Frau, F., 2015. Stable isotope data as constraints on models for the origin of coralloid and massive speleothems: the interplay of substrate, water supply, degassing, and evaporation. Sedimentary Geology, 318, 130-141. https://doi.org/10.1016/j.sedgeo.2014.12.008

Chiesi, M., Forti, P., 1987. Studio morfologico di due nuove cavitá carsiche dell'Iglesiente (Sardegna Sud occidentale). Ipoantropo, 4, 40-45.

D'Angeli, I.M., De Waele, J., Melendres, O.C., Tisato, N., Sauro, F., Gonzales, E. Grau, R., Stefano, B., Torriani, M., Stefano, T., Bontognali, R.R., 2015. Genesis of folia in a non-thermal epigenic cave (Matanzas, Cuba). Geomorphology, 228, 526-535. https://doi.org/10.1016/j.geomorph.2014.09.006

Davis D.G., 1997. Folia in Hurricane Crawl Cave and Crystal Sequoia Cave. San Francisco Bay Chapter Newsletter, 40(5), 3-7. https://doi.org/10.5038/k26.5679

Davis, D.G., 2012. In defense of a fluctuating-interface, particle-accretion origin of folia. International Journal of Speleology, 41(2), 189-198. https://doi.org/10.5038/1827-806X.41.2.6

Daza, R., Bustillo, M.A, 2014. Exceptional silica speleothems in a volcanic cave: A unique example of silicification and sub-aquatic opaline stromatolite formation (Terceira, Azores). Sedimentology, 61, 2113-2135. https://doi.org/10.1111/sed.12130

De Waele J., Forti P., 2006. A new hypogean karst form: the oxidation vent. Zeitschrift für Geomorphologie, Supplementary Issue 147, 107-127.

De Waele, J., D'Angeli, I.M., Bontognali, T., Tuccimei, P., Scholz, D., Jochum, K. P., Colombus, A., Bernasconi. M.S., Fornos, J.J., Grau, E.R., Tisato, N., 2018. Speleothems in a north Cuban cave register sea-level changes and Pleistocene uplift rates. Earth Surface Processes and Landforms, 43(11), 2313-2326. https://doi.org/10.1002/esp.4393

De Waele, J., D'Angeli, I.M., Tisato, N., Tuccimei, P., Soligo, M., Ginés, J., Bernasconi, S.M., 2017. Coastal uplift rate at Matanzas (Cuba) inferred from MIS 5e phreatic overgrowths on speleothems. Terra Nova, 29(2), 98-105. https://doi.org/10.1111/ter.12253

Dickson, J.A.D., 1993. Crystal growth diagrams as an aid to interpreting the fabrics of calcite aggregates. Journal of Sedimentary Research, 63(1), 1-17. https://doi.org/10.1306/D4267A78-2B26-11D7-8648000102C1865D

Frisia, S., 2014. Microstratigraphic logging of calcite fabrics in speleothems as a tool for palaeoclimate studies. International Journal of Speleology, 44(1), 1-16. https://doi.org/10.5038/1827-806X.44.1.1

Frisia, S., Borsato, A., Fairchild, I.J., McDermott, F., 2000. Calcite fabrics, growth mechanisms, and environments of formation in speleothems from the Italian Alps and southwestern Ireland. Journal of Sedimentary Research, 70(5), 1183-1196. https://doi.org/10.1306/022900701183

Gázquez, F., Calaforra, J.M., 2013. Origin of double-tower raft cones in hypogenic caves. Earth Surfaces Process and Landforms, 38, 1655-1661. https://doi.org/10.1002/esp.3399

Green, D.J., 1991. On the origin of the folia and rims. Salt Lake Grotto Technical Note 88, Salt Lake Grotto, National Speleological Society, 182-196.

Green, D.J., 1997. The origin of folia. Salt Lake Grotto Technical Note 96, Salt Lake Grotto, National Speleological Society, 51-60.

Gulley, J.D., Martin, B.J., Brown, A., 2016. Organic carbon inputs, common ions and degassing: rethinking mixing dissolution in coastal eogenetic carbonate aquifers. Earth Surface Processes and Landforms, 41(14), 2098-2110. https://doi.org/10.1002/esp.3975

Hill, C.A., Forti, P. 1997. Cave minerals of the world (2nd Ed.). National Speleological Society, Huntsville, 463 p.

Hose, L., 2009. Recent observations in a remarkably dynamic, sulfide-rich, hypogenic cave in southern Mexico. Proceedings of the 15th International Congress of Speleology, 3, 1525-1530.

Hose, L.D., Palmer, A.N., Palmer, M.V., Northup, D.E., Boston, P.J., DuChene, H.R., 2000. Microbiology and geochemistry in a hydrogen-sulphide-rich karst environment. Chemical Geology 169, 399-423.

Jones, B., 2001. Microbial activity in caves − A geological perspective. Geomicrobiology Journal, 18(3), 345-357. https://doi.org/10.1080/01490450152467831

Jones, B., Kahle, C.F., 1995. Origin of endogenetic micrite in karst terrains; a case study from the Cayman Islands. Journal of Sedimentary Research, 65(2), 283-293. https://doi.org/10.1306/D426809F-2B26-11D7-8648000102C1865D

Kendall, A.C., Broughton, P.L., 1978. Origin of fabrics in speleothems composed of columnar calcite crystals. Journal of Sedimentary Research, 48(2), 519-538. https://doi.org/10.1306/212F74C3-2B24-11D7-8648000102C1865D

Kendall, A.C., 1993. Columnar calcite in speleothems: discussion. Journal of Sedimentary Research, 63(3), 550-552. https://doi.org/10.1306/D4267B54-2B26-11D7-8648000102C1865D

Kolesar, P.T., Riggs, A.C., 2004. Influence of depositional environment on Devils Hole calcite morphology and petrology. In: Sasowsky, I.D., Mylroie, J. (Eds.), Studies of cave sediments. Kluwer Academic/Plenum Publishers, New York, p. 227-241. https://doi.org/10.1007/978-1-4419-9118-8_12

Kovacs, S.E., Reinhardt, E.G., Stastna, M., Coutino, A., Werner, C., Collins, S.V., Le Maillot, C., 2017a. Hurricane Ingrid and Tropical Storm Hanna's effects on the salinity of the coastal aquifer, Quintana Roo, Mexico. Journal of Hydrology, 551, 703-714. https://doi.org/10.1016/j.jhydrol.2017.02.024

Kovacs, S.E., Reinhardt, E.G., Chatters, J.C., Rissolo, D., Schwarcz, H.P., Collins, S. V., Luna Erreguerena, P., 2017b. Calcite raft geochemistry as a hydrological proxy for Holocene aquifer conditions in Hoyo Negro and Ich Balam (Sac Actun Cave System), Quintana Roo, Mexico. Quaternary Science Reviews, 175, 97-111. https://doi.org/10.1016/j.quascirev.2017.09.006

López-Martínez, R., Barragán, R., Beraldi-Campesi, H., Lánczos, T., Vidal-Romaní, J.R., Aubrecht, R., Espinasa-Pereña, R., 2016. Morphological and mineralogical characterization of speleothems from the Chimalacatepec lava tube system, Central Mexico. International Journal of Speleology, 45(2), 111-122. https://doi.org/10.5038/1827-806X.45.2.1927

López, R., 1983. Estudio geológico de la Península de Yucatán. Boletín Asociación Mexicana de Geólogos Petroleros, 25(1-3), 23-76.

Lugli, S., Rosario, R., Riccardo, O., Giorgio, S., 2017. Grotta dell'Acqua Mintina, a peculiar geosite with the smell of sulfur. Speleologia Iblea, XVI, 65-71. https://iris.unimore.it/retrieve/handle/11380/1129517.1/130489/Lugli%20et%20al%202017%20Speleologia%20Iblea.pdf;jsessionid=62EAE2D18407C42C0A995363D4B6B4B4.suir-unimore-prod-02

Luis-Vargas, M.N., López-Martínez, R., Vilchis-Nestor, A.R., Daza, R., Alcántara-Hernández, R.J., 2019. Bacterial insights into the formation of opaline stromatolites from the Chimalacatepec Lava Tube System, Mexico. Geomicrobiology Journal, 36(8), 694-704. https://doi.org/10.1080/01490451.2019.1607952

Martín-Chivelet, J., Muñoz-García, M.B., Cruz, J.A., Ortega, A.I., Turrero, M.J., 2017. Speleothem architectural analysis: Integrated approach for stalagmite-based paleoclimate research. Sedimentary Geology, 353, 28-45. https://doi.org/10.1016/j.sedgeo.2017.03.003

Martínez-Yáñez, M., Núñez-Useche, F., Martínez, R.L., Gardner, R.D., 2017. Paleoenvironmental conditions across the Jurassic–Cretaceous boundary in central-eastern Mexico. Journal of South American Earth Sciences, 77, 261-275. https://doi.org/10.1016/j.jsames.2017.05.007

Núñez-Useche, F., Canet, C., Barragán, R., Alfonso, P., 2016. Bioevents and redox conditions around the Cenomanian–Turonian anoxic event in Central Mexico. Palaeogeography, Palaeoclimatology, Palaeoecology, 449, 205-226. https://doi.org/10.1016/j.palaeo.2016.01.035

Plan, L., De Waele, J., 2011. Folia in der Oedelsteinhöhle, Steiermark. Erstnachweis im deutschsprachigen Raum. Die Höhle, 62, 54-57.

Queen, M., 2009. The Lost City: hot springs, mixing and a possible model for folia development. Proceedings of the 15th International Congress of Speleology, 3, 1650-1656.

Railsback, L.B., Akers, P.D., Wang, L., Holdridge, G.A., Voarintsoa, N.R., 2013. Layer-bounding surfaces in stalagmites as keys to better paleoclimatological histories and chronologies. International Journal of Speleology, 42(3), 167-180. https://doi.org/10.5038/1827-806X.42.3.1

Ritter, S.M., Isenbeck-Schröter, M., Scholz, C., Keppler, F., Gescher, J., Klose, L., Stinnesbeck, W., 2019. Subaqueous speleothems (Hells Bells) formed by the interplay of pelagic redoxcline biogeochemistry and specific hydraulic conditions in the El Zapote sinkhole, Yucatan Peninsula, Mexico. Biogeosciences, 16(11), 2285-2305. https://doi.org/10.5194/bg-16-2285-2019

Smart, P.L., Beddows, P.A., Coke, J., Doerr, S., Smith, S., Whitaker, F.F., 2006. Cave development on the Caribbean coast of the Yucatan Peninsula, Quintana Roo, Mexico. Geological Society of America, Special Paper, 404, 105-128. https://doi.org/10.1130/2006.2404(10)

Stinnesbeck, S.R., Frey, E., Olguín, J.A., Stinnesbeck, W., Zell, P., Mallison, H., Gonzalez, A., Aceves, E., Morlet, A., Terrazas, A., Sanvicente, M.B., Hering, F., Rojas-Sandoval., C., 2017. Xibalbaonyx oviceps, a new megalonychid ground sloth (Folivora, Xenarthra) from the Late Pleistocene of the Yucatán Peninsula, Mexico, and its paleobiogeographic significance. PalZ, 91(2), 245-271. https://doi.org/10.1007/s12542-017-0349-5

Stinnesbeck, W., Frey, E., Zell, P., Avilés, J., Hering, F., Frank, N., Arps, J., Geenen, A., Isenbeck- Schröter, M., Ritter, S., Stinnesbeck, S., Aceves, E., Fito, V., Gonzales, A., Deininger, M., 2018. Hells Bells–unique speleothems from the Yucatán Peninsula, Mexico, generated under highly specific subaquatic conditions. Palaeogeography, Palaeoclimatology, Palaeoecology, 489, 209-229. https://doi.org/10.1016/j.palaeo.2017.10.012

Stoessell, R.K., Moore, Y.H., Coke, J.G., 1993. The occurrence and effect of sulfate reduction and sulfide oxidation on coastal limestone dissolution in Yucatán cenotes. Groundwater, 31(4), 566-575. https://doi.org/10.1111/j.1745-6584.1993.tb00589.x

van Beynen, P., Bourbonniere, R., Ford, D., Schwarcz, H., 2001. Causes of colour and fluorescence in speleothems. Chemical Geology, 175(3-4), 319-341. https://doi.org/10.1016/S0009-2541(00)00343-0

Veress, M., 2010. Karst environments: karren formation in high mountains. Springer, Dordrecht, 230 p.

Vidal-Romaní, J.R., González-López, L., Vaqueiro, M., Sanjurjo-Sánchez, J., 2015. Bioweathering related to groundwater circulation in cavities of magmatic rock massifs. Environmental Earth Sciences, 73(6), 2997-3010. https://doi.org/10.1007/s12665-014-3743-2

Ward, W.C., Weidie, A.E., Back, W., 1985. Geology and hydrogeology of the Yucatan and Quaternary Geology of northeastern Yucatan Peninsula. New Orleans Geological Society, New Orleans, 119 p.

Ward, W., Keller, G., Stinnesbeck, W., Adatte, T., 1995. Yucatan subsurface revisited: Implications and constraints for the Chicxulub Meteor Impact. Geology, 23, 873-876. https://doi.org/10.1130/0091-7613(1995)023%3C0873:YNSSIA%3E2.3.CO;2

Wignall, P.B., Bond, D.P., Kuwahara, K., Kakuwa, Y., Newton, R.J., Poulton, S.W., 2010. An 80 million year oceanic redox history from Permian to Jurassic pelagic sediments of the Mino-Tamba terrane, S.W. Japan, and the origin of four mass extinctions. Global and Planetary Change, 71(1-2), 109-123. https://doi.org/10.1016/j.gloplacha.2010.01.022

Wilkin, R.T., Barnes, H.L., 1997. Pyrite formation in an anoxic estuarine basin. American Journal of Science, 297(6), 620-650. https://doi.org/10.2475/ajs.297.6.620